Analiza difuzije integrina alfa5beta1 metodom praćenja na razini jedne molekule

Ivčević, Jelena

UNIVERSITY OF ZAGREB

FACULTY OF SCIENCE

Department of Biology

Jelena Ivčević

ANALYSIS OF α5β1 INTEGRIN DIFFUSION WITH SINGLE-PARTICLE TRACKING

Master thesis

Zagreb, 2019.

This thesis was made at the Faculty of Science and Technology of the University of Vic in Spain, under the supervision of dr.sc. Carlo Manzo. The thesis has been submitted for grading to the Department of Molecular Biology of Faculty of Science of University of Zagreb, for the purpose of acquisition of Master's degree in Molecular Biology.

TEMELJNA DOKUMENTACIJSKA KARTICA

Sveučilište u Zagrebu
Prirodoslovno-matematički fakultet
Biološki odsjek

ANALIZA DIFUZIJE INTEGRINA α5β1 METODOM PRAĆENJA NA RAZINI JEDNE MOLEKULE

Jelena Ivčević

Rooseveltov trg 6, 10000 Zagreb, Hrvatska

SAŽETAK

U ovom radu implementirana je metoda proučavanja lateralnog gibanja integrina α5β1 na razini jedne molekule. Integrini su transmembranski, glikoproteinski heterodimeri, najvećim dijelom odgovorni za procese usidrenja, adhezije i migracije stanice. Lateralna difuzija integrina na membrani važan je aspekt stanične adhezije i mobilnosti, a njen utjecaj na stanične biokemijske i biomehaničke procese još uvijek nije detaljno istražen. Kvantificiranje gibanja proteina membrane stanice i razlučivanje njihove biološke funkcije uvelike je unaprijeđeno razvojem metode praćenja na razini jedne molekule (SPT od engl. Single-Particle Tracking). SPT se sastoji od obilježavanja ciljane molekule niskom koncentracijom reportera, snimanja video-zapisa mikroskopom i obrade slika složenim algoritmima koji nanometarskom preciznošću lociraju individualne molekule te povezuju njihovo gibanje u putanje. Razumijevanje složenog gibanja na razini molekule potencijalno može doprinijeti razvijanju terapijskih postupaka za stanja povezana s disfunkcijom integrina, poput kožnih rana ili metastaziranja tumora. Glavni cilj ovog istraživanja je stoga bio implementirati i optimizirati SPT-metodu za mjerenje difuzije integrina α5β1. Difuzija integrina obilježenih s reduciranim poluantitijelom uspoređena je s difuzijom integrina obilježenih klasičnim cjelovitim antitijelom, kako bi se utvrdilo utječe li imunoobilježavanje na gibanje integrina zbog dimerizacije i stvaranja umjetnih klastera. Utvrđena je statistički značajna razlika u distribuciji koeficijenata difuzije između dva tipa obilježenih integrina.

(42 stranica teksta, 18 slika, 8 tablica, 38 literaturnih izvora, jezik izvornika: engleski)
Rad je pohranjen u Središnjoj biološkoj knjižnici.
Ključne riječi: praćenje na razini jedne molekule, lateralna difuzija, integrini

Voditelj: Dr.sc. Carlo Manzo, red. prof.
Suvoditelj: Dr. sc. Petra Korać, izv. prof.

Ocjenitelji: Dr. sc. Petra Korać, izv. Prof
Dr. sc. Renata Šoštarić, izv. Prof
Dr. sc. Duje Lisičić, doc.

Rad prihvaćen: 18.09.2019.

BASIC DOCUMENTATION CARD

University of Zagreb
Faculty of Science
Division of Biology

Graduation Thesis

ANALYSIS OF α5β1 INTEGRIN DIFFUSION WITH SINGLE PARTICLE TRACKING

Jelena Ivčević

Rooseveltov trg 6, 10000 Zagreb, Croatia

ABSTRACT

In this thesis, a method for studying lateral mobility of integrin α5β1 on a single-molecule level was set up and applied. Integrins are transmembrane, heterodimeric glycoproteins, mainly responsible for the processes of cell anchoring, adhesion, and migration. Lateral diffusion of integrins on the membrane is an important aspect of the cell adhesion and mobility, but how it affects the cell's biochemical and biomechanical processes is still not thoroughly investigated. Quantifying movement of membrane proteins and elucidating their biological function has greatly been improved with Single-Particle Tracking (SPT). SPT is based on the sparse labeling of the target molecule, recording the movement of particles in a series of videos by optical microscopy and analysis of videos by image-processing algorithms that locate individual molecules with nanometric precision and establish a correspondence between particles in each frame. Understanding integrin's complex behavior at the single-molecule level could potentially lead to the development of treatments for conditions linked to integrin-dysfunction such as injury or cancer. The objective of this thesis was to implement and optimize the SPT method for studying the diffusion of α5β1 integrin at the single-molecule level. Diffusion of integrins labeled with the reduced half-antibody fragment was compared to those labeled with the whole antibody to test if the immuno-labeling is influencing integrin movement through dimerization and artificial clustering. A statistically significant difference in the distribution of two types of labeled integrins was determined.

(42 pages, 18 figures, 8 tables, 38 references, original in English)
Thesis deposited in Central biological library.
Keywords: Single-Particle Tracking, lateral diffusion, integrins

Supervisor: Dr.sc. Carlo Manzo, Prof.
Co-supervisor: Dr.sc. Petra Korać, Assoc. Prof

Reviewers: Dr. sc. Petra Korać, Assoc. Prof
Dr. sc. Renata Šoštarić, Assoc. Prof
Dr. sc. Duje Lisičić, Doc.

Thesis accepted: 18.09.2019.

CONTENTS

1. INTRODUCTION

1.1. HUMAN DERMOFIBROBLAST CELLS

Most abundant cell type present in the body's connective tissue are fibroblasts (Sriram, Bigliardi, and Bigliardi-Qi 2015). Fibroblasts are of mesenchymal origin and provide a structural framework and mechanical support in animal tissues. They are conventionally characterized by spindle-shaped morphology, adhesive growth on cell-culture plastic and by their role in synthesizing components of the extracellular matrix (ECM). Their typical morphology in cell culture is shown in Figure 1. Along with the role in protein synthesis of ECM components, they contribute to many other vital processes in the cell such as epithelial differentiation, regulation of inflammation, and wound healing (Rodemann and Müller, 1991; Tomasek et al., 2002). Recently, multiple studies are making effort to elucidate their role in cancer development and progression (Guo et al. 2002; Noda et al. 1999; Erez et al. 2010). Their vast heterogeneity and vital importance for multiple biological processes make them excellent research topic, even more so because fibroblasts are among the most accessible and undemanding normal mammalian cell types.

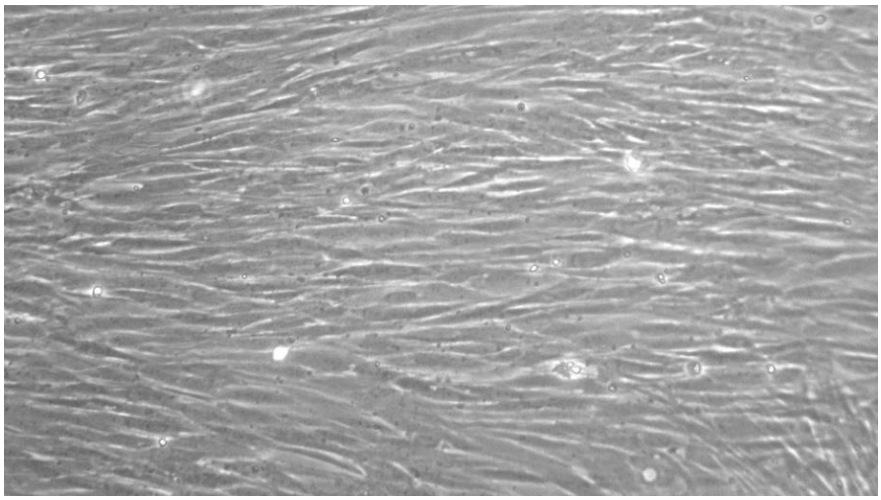

Figure 1. Fibroblasts monolayer in cell culture. They are spindle-shaped and attach well to cell culture plastics. In this example, cells are 100% confluent (they cover all the substrate surface).

1.2. INTEGRINS

Fibroblasts are attached to the substratum in the areas called focal contacts. At focal contacts, actin filaments are connected to the ECM through transmembrane glycoproteins in the plasma membrane which form focal adhesion plaques. Focal adhesions are multi-protein structures that not only serve as a cell's anchoring to the ECM but also as signal carriers. They receive signals from the ECM and by changing conformation and reorganizing the actin cytoskeleton, direct the cell's response (Alberts et al. 2017).

Transmembrane glycoproteins that can be found at focal adhesions belong to the family of integrins. Integrins are heterodimers, consisting of two subunits α and β. 8 β-subunits bind with 18 α subunits to form 24 distinct combinations (Hynes 2002), shown in Figure 2. Each subunit contains a large external glycosylated portion which binds them to ECM components, a transmembrane domain, and a short cytoplasmic stretch of amino acids at the C terminus which binds to adaptor proteins connected to the actin cytoskeleton (Nermut et al. 1988). As shown in Figure 2., the largest subgroup of integrins is integrin β_1, connecting with 12 different α subunits. β_1 integrin binds to many different ligands, such as collagen, laminin, and fibronectin (Hynes 2002).

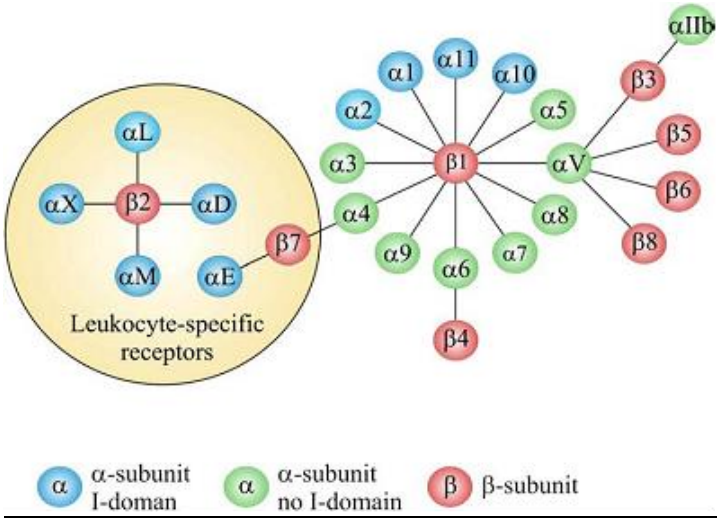

Figure 2. Twenty-four distinct integrin heterodimers as a result of combinations between 8 β and 18 α subunits. Adapted from Niu and Chen 2012.

Participating in signal transduction, they play a vital role in many of the cell processes such as cell differentiation, survival/apoptosis, proliferation, motility and others (Hynes, 2002). An example of integrin with such importance for cell viability and development is α5β1 integrin, investigated in this thesis. It binds to the fibronectin (FN)– a protein present in the ECM as a polymeric fibrillar network that serves as a cell's attachment point (Figure 3). Mice with an inactivated fibronectin gene or α5 subunit-deficient mice die at early embryonic stages (George et al., 1993; Goh, Yang, and Hynes, 1997). α5β1-FN binding mediates adhesion, migration, assembly of a cytoskeleton and assembly of the fibronectin extracellular matrix (Akiyama et al., 1989). It also participates in tumor-cell survival, proliferation, and metastasis (Akiyama, Olden, and Yamada, 1995; Danen and Yamada, 2001).

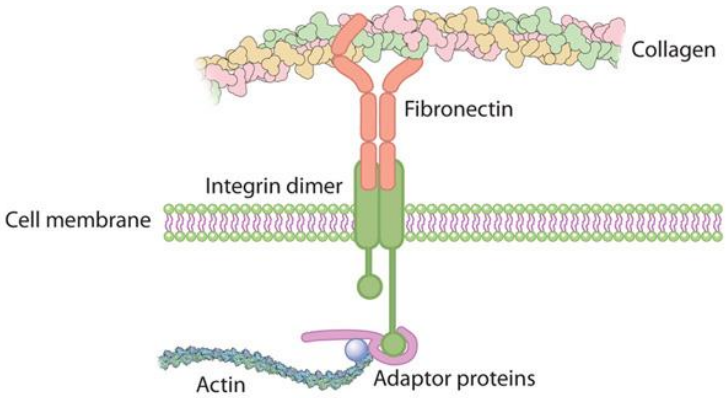

Figure 3. Integrins connect extracellular matrix with the actin cytoskeleton inside the cell. α5β1 integrin binds fibronectin, ECM protein that serves as a cell's attachment point. Adapted from ©Nature Education.

An important aspect of cell adhesion and motility is the lateral diffusion of integrins on the membrane (Miyamoto et al., 1995; Rossier et al., 2012). Nowadays, the cell membrane is recognized as a highly dynamic and compartmentalized structure. The membrane structure has been described in detail from a static point of view, but the dynamics of proteins on the membrane is still not fully investigated and it is a step towards understanding their biological functions. For this reason, integrin movement has been widely studied but how it affects cell biochemical and biomechanical processes is still not thoroughly investigated. Understanding this complex behavior at the single-molecule level could potentially lead to the development of treatments for conditions linked to integrin-dysfunction, such as skin injury or cancer metastasis.

1.3. SINGLE-PARTICLE TRACKING

Quantifying different types of heterogeneous movement of membrane proteins and elucidating their biological function has greatly been improved with Single-Particle Tracking (SPT) (Kusumi et al. 2005). SPT is a method used to quantify protein movement on the surface of living cells. SPT experiments are based on the sparse labeling of the target protein with a nanoscopic reporter. After labeling, cells are imaged by optical microscopy and the motion of the reporter is recorded in a series of movies. Each movie is a sequence of images (frames) in time. Recorded movies are then analyzed by image-processing algorithms that reconstruct the trajectories of labeled particles.

A great deal of techniques have been developed for measuring dynamic processes in living cells, some of which are widely used such as fluorescence recovery after photobleaching (FRAP) and fluorescence correlation spectroscopy (FCS). While these and similar techniques provide information on the mobility of large ensemble of molecules, SPT on the other hand is capable of visualizing movement of individual fluorescently labeled molecules as a function of time. This in turn gives access to dynamic fluctuations and nanoscale heterogeneity of molecules in the cell. Based on optical microscopy, SPT is a method with limited invasiveness and allows for exploration of the movement of the particles in the natural context of the living cells. Furthermore, the position of the particles can be determined with a precision that exceeds microscope resolution limit, at the nanometer scale. SPT algorithms perform not only the localization of the particles but importantly, they establish a correspondence between particles in each frame. With improvements in reporter design and in image-processing algorithms, distinct molecules can be tracked for a relatively long period of time. All factors combined mean that subcellular events in living cells can be determined with high spatiotemporal resolution. This depends mainly on photophysical properties of the chosen reporter, detector speed and signal-to-noise ratio (Manzo and Garcia-Parajo 2015).

Reporters can be non-fluorescent (most often gold particles), and fluorescent particles which include organic dyes, autofluorescent proteins, and Quantum Dots (QDs). Larger reporters (gold particles) usually have better optical performance than smaller (organic dyes), but tend to alter biomolecule natural behavior in the cell and induce artifacts. QDs are a compromise between size and optical properties. They are inorganic semiconductor nanocrystals. Their inorganic cores are small in size, in the range of 4-10 nm in diameter, but

to render them functional and stable, outer layers must be added which results in size up to 30 nm. The emission wavelength is tunable by the size of the crystal. Larger than other fluorescent particles but smaller than gold particles, their size might still affect molecule behavior (Groc et al. 2007). On the other hand, they have excellent optical performance, far surpassing organic dyes and fluorescent proteins. Optical properties include wide absorption cross-section and a large molar extinction coefficient. Having wide absorption spectra and narrow emission band, it is possible to simultaneously excite multiple fluorescence colors which is why QDs are widely used in multi-color SPT experiments. Moreover, they are orders of magnitude more stable than organic dyes and fluorescent proteins. As a result, molecules can be tracked for much longer observation time. Development of surface coating and bio-conjugation protocols made them an excellent choice for experiments on living cells.

QDs disadvantage is the phenomenon of "blinking" or intermittent fluorescence first observed by Nirmal *et al.*, 1996. Put simply, individual QDs alternate between "on", bright state and "off" dark state. This makes them very recognizable when imaging, but in SPT experiment, because spots can be in "off" state for several frames, blinking causes difficulties with algorithm trying to reconstruct trajectories. In practice, false reconnections and mixing of trajectories can be minimized (although not resolved) by using a low concentration of QDs.

Existing algorithms that process raw data can be divided into two parts, algorithms for particle localization and for particle linking. Particles in collected images appear as Airy pattern that is, as a light diffraction pattern of decaying concentric rings. In the center of the ring is a bright spot that contains most of the particle intensity, called Airy disk. One option for particle localization is fitting the intensity profile of the disk with a 2D spatial Gaussian, which in practice works well for isotropic points (Manzo and Garcia-Parajo 2015), using this equation:

$$I(x,y) \approx I_0 exp\left\{-\frac{(x-x_0)^2}{2w^2}\right\} exp\left\{-\frac{(y-y_0)^2}{2w^2}\right\}.$$

I_0 is the intensity at the center of the disk, x and y are coordinates at the edge, x_0, and y_0 at the center, and w is a standard deviation of the intensity profile. The intensity profile is also known as point spread function (PSF) of the microscope. Graphical illustration of Gaussian PSF is shown in Figure 4. Full-width-at-half-maximum (FWHM) is the width of a fluorescent object at the point where its intensity is half of the maximum. Because of the diffraction limit of light, two particles cannot be resolved if their mutual distance is less than FWHM. As mentioned above, the way to overcome this is to use sparse labeling conditions. In this way,

particles are well separated in the sample and their FWHMs do not overlap so their centroid position can be estimated to a nanometer.

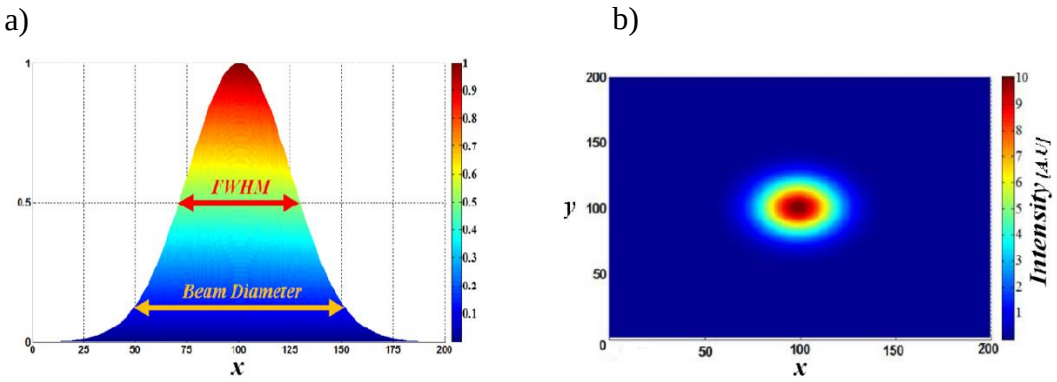

Figure 4. Intensity profile i.e. Gaussian point spread function (PSF) of the microscope, viewed from the side (a) and viewed from the above (b). In (a) full-width-at-half-maximum (FWHM) is shown – if the FWHM of the two particles overlaps, they cannot be distinguished from one another. Adapted from Ahi and Anwar (2016.)

After localizing particles in each frame follows particle linking i.e. connecting detected particles from frame to frame using a specific set of criteria. Linking particles is not trivial since some particles can be mislocalized in some frames, go out of the frame or photobleach. Another set of problems comes from two or more particles crossing paths, aggregating or being too close so they cannot be resolved from one another. Sophisticated algorithms are needed to perform tracking and deal with the described problems. A schematic example of how localization and tracking are performed is shown in Figure 5.

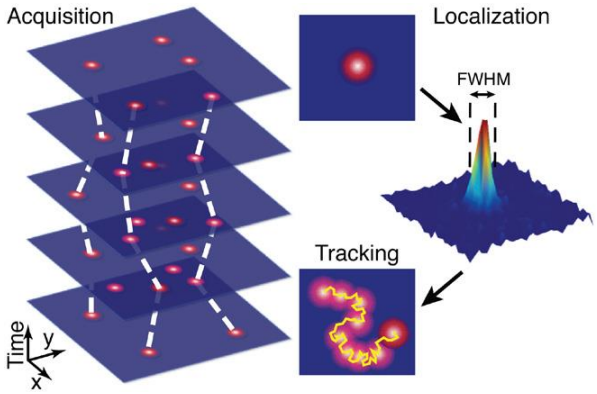

Figure 5. A schematic representation of SPT localization and tracking. Particles that can be resolved (if their FWHMs don't overlap, which is achieved by sparse labeling) are first localized in each frame then connected in trajectories. Adapted from Manzo and Garcia-Parajo, (2015.)

Often a lot of noise from the sample comes from autofluorescence. To reduce noise and consequently improve the signal-to-noise ratio, the key is to use the smallest illumination volume possible. With classic wide-field illumination, laser beam excites a region of the sample throughout the entire sample depth. Total-internal-reflection microscopy (TIRM or in the case of fluorescence microscopy TIRFM) is used to achieve illumination of the smaller portion of the sample depth. In the case of two media with different refractive indices, such as a glass of the coverslip and water, the laser beam is partially diffracted and partially reflected at their interface. At the specific angle, called critical angle, light is completely reflected and this phenomenon is called total-internal-reflection fluorescence. Now the illumination depth is limited by the penetration of the evanescent field through the sample, which is up to ~200nm from the interface. Normally basal membrane is in contact with the glass surface which is why TIRFM is specifically suitable for cell membrane studies.

Finally, SPT results are trajectories that are obtained from the movement of the particle labeled with the reporter. From trajectories, different motion parameters can be derived such as displacement, velocity, and acceleration (Meijering, Smal, and Danuser 2006). Data is usually processed over hundreds of particles, then represented together as a histogram that shows main types of molecule behavior. Motion parameter widely used to characterize particle's movement is mean squared displacement (MSD). From this parameter, the diffusion coefficient of integrins can be determined. Particles movement can be divided into different types, e.g. immobile, directed, confined, normal diffusion or anomalous diffusion (Saxton and Jacobson, 1997), by plotting MSD curve as a function of time lag.

In the experiments conducted in this study, the stage is set for detailed analysis of the diffusion of integrins under different experimental conditions, by means of high-resolution Single-Particle Tracking experiments. Preferentially reduced half-antibody fragments (one heavy and one light chain) are nowadays promising in labeling applications (Hermanson 2007; Makaraviciute et al. 2016) and were used to label integrins. Since unreduced antibody that has two antigen-binding sites can theoretically bind two integrins at once and induce artificial dimerization, it might affect the diffusion rate of molecules. To investigate this, integrins were labeled with reduced fragments and unreduced antibody and their diffusion compared. Experiments were repeated on different cell passages to observe if cell senescence is responsible for changes in diffusion.

1.4. OBJECTIVES OF THE EXPERIMENT

1. Implement and optimize the method for obtaining diffusion coefficients of α5β1 integrin on human dermal fibroblasts with Single-Particle Tracking.
2. Measure diffusion on fixed cells to obtain a reference for localization precision.
3. Measure diffusion on cells labeled with reduced and with unreduced antibody to take into account the antibody's influence on the movement.
4. Measure diffusion on fibroblasts of different passage number to take into account "cell senescence".
5. Determine the potential difference of diffusion coefficients in different conditions.

2. MATERIAL AND METHODS

2.1. CELL CULTURE

For this study, cell culture of human dermofibroblasts HFF-1 taken from male foreskin (ATCC®, Ref. SCRC-1041™) was established and maintained. It is an adherent culture with a finite lifespan (non-immortalized). Primary fibroblast cell cultures can be easily established, they proliferate rapidly and there is no requirement for specialized medium or activation protocols. Primary cells in culture undergo replicative senescence and cultures need to be re-established during the time, although fibroblasts can be passed to a new generation a substantial number of times before senescence occurs. Normal HFF-1 cells in culture express different types of integrins on the cell membrane, among which is α5β1. Before use, cells were thawed following the protocol provided by the ATCC. Culture hood and all materials were rigorously kept sterilized with 70% ethanol and UV-light. Cells were mainly grown in T25 flasks in complete medium DMEM (Gibco™, Ref. 11960-044) complemented with 15% Fetal Bovine Serum FBS (SIGMA, F0679), Penicillin-Streptomycin (10,000 U/mL, Gibco™, Ref. 15140122) and 200 mM L-Glutamine solution (SIGMA, Ref. G7513).

When cells would reach 80-90% confluency, approximately each 2-4 days, they would be split into two new T25 flasks in the following way: first, PBS, medium and trypsin were warmed up to 37°C, old media removed using vacuum aspiration pump with glass tip, then the flask was washed 2x with 3 ml Phosphate-buffered saline (PBS) using pipettor, after which 1-1.5 ml (depending on the confluency) of trypsin was added. After verifying on the invert-microscope that the cells have detached, the same amount of media was added to neutralize trypsin, solution extensively homogenized and 1-1.5 ml passed to each of the two new flasks. Media was added up to the total volume of 6 ml and flasks put into the incubator (37°C, 5% CO_2). Cell counting was performed in the Neubauer chamber. 50 µl of the sample was taken before splitting the cell solution to new flasks and mixed with 50 µl of Trypan blue dye. Cells were counted under invert-microscope.

2.2. SAMPLE PREPARATION

2.2.1. Glass coating with fibronectin and seeding cells

35 mm glass-bottom dishes suitable for inverted-microscope observation were used in all experiments. Glass was coated with fibronectin, a glycoprotein found in the ECM that binds to α5β1 integrin. Fibronectin coating promotes attachment and proliferation of fibroblasts. Each tube contained 8 µl of fibronectin solution, and 4 µl per plate was required in a sufficient volume of sterile water to cover all the glass surface. Therefore, each tube was enough for coating of two dishes. With a micropipette, 192 µl sterile water (warmed up to 37°C) was added to the tube and homogenized. Then the content was transferred to 1ml tube and 400 µl more of sterile water was added, after which the solution was homogenized and pipetted 300 µl per dish, making sure that the whole circle of glass was covered. Then dishes were incubated 1h at 37°C. After incubation, whole solution was removed, being careful not to touch the glass bottom, and 500 µl albumin solution was pippeted per dish and returned to the incubator for 1h. Afterward, the solution was again removed and dishes were ready for seeding the cells or if they weren't needed immediately, they were taped with parafilm and stored in the fridge (4°C).

Cells were seeded on plates after trypsinization protocol described in section 2.1., in volumes depending on the confluency observed, and on the date of planned experiments, usually from 0.1-0.7 ml per plate. Then the media would be added up to 2 mL. It's important to note that in this case, DMEM without phenol red was used, since this pH-indicator increases background fluorescence which could interfere with QD fluorescence.

2.2.2. Antibody biotinylation

Purified Mouse Anti-Human CD49e (BD Pharmingen™, Ref. 555651) that binds to the α5 integrin subunit was used as a primary antibody in all experiments, either in its intact form or reduced to half-antibody (hAb) fragments (Hermanson 2007). This clone does not inhibit ligand binding to α5β1. It is an Immunoglobulin G (IgG) type of antibody, composed of two light and two heavy chains. Heavy chains are connected with disulfide bonds in the hinge

region. The reduction of bonds in the hinge region yields two half-antibody (hAb) molecules, each containing one light and one heavy chain, with only one antigen-binding region per hAb (Figure 6). Antibody reduction was carried out by the laboratory group before the start of my thesis and hAb fragments were ready to use.

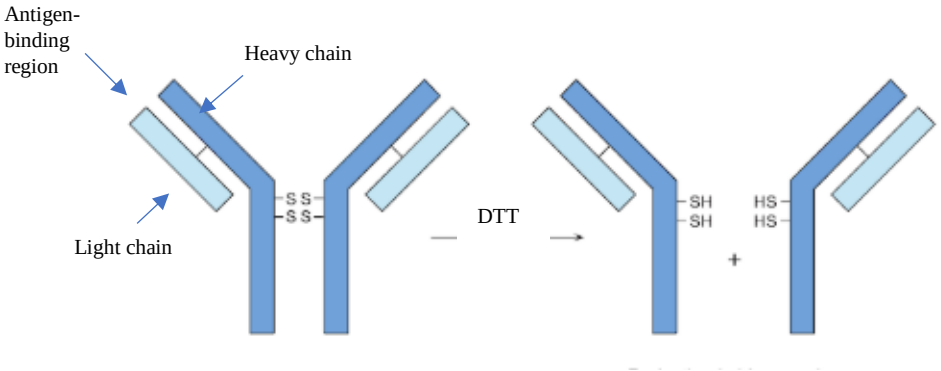

Figure 6. Reduction of immunoglobulin G antibody in the hinge region yields two half-antibodies, each with one heavy and one light chain and one antigen-binding place. Reduction in the hinge region can be produced with reducing agents such as dithiothreitol (DTT). Adapted from Hermanson, 2007.

To be suitable for detection using streptavidin-coated QDs (Qdot™ 655 Streptavidin Conjugate, Ref. Q10121MP), the antibody was biotinylated using EZ-Link™ Sulfo- N-Hydroxysuccinimide (NHS) -Biotin (Thermo Scientific™, Ref. A39256). Biotin is a water-soluble molecule that binds with high affinity to streptavidin and avidin probes. It is also very small (244 Da) and it can be conjugated to proteins without affecting their biological activity. Sulfo-NHS esters of biotin react with primary amino groups (-NH2) and form stable amide bonds. They are not membrane permeable and are used for labeling of cell surface proteins.

Biotinylation was carried out following the manufacturer's recommended protocol. For biotinylated proteins diluted in solution, greater fold molar excess of biotin reagent is required. In this case, 10-fold molar excess was used. Knowing the whole antibody (wAb) concentration is 0.5 mg/ml and hAb fragments 0.180 mg/ml, the number of moles of each was calculated in the total volume that was set to 50 µl. Then the volume of E-Z link that needs to be taken to have 10x more moles than the antibody was calculated which was 0,12 µl for hAb and 0.17 µl for wAb. Since these volumes were below the sensitivity level of laboratory pipettes, E-Z link was diluted 10x, by mixing 50 µl with 450 µl of ultrapure water. Then 1,2 µl of E-Z link was

mixed in 50 µl of hAb solution in one tube, and 1,7 µl of E-Z link in 50 µl of wAb solution in the other. Biotinylated antibodies were stored at 4°C.

2.2.3. Antibody conjugation with Quantum Dots coated with streptavidin

In the next step of sample preparation, biotinylated antibodies were joined with Quantum Dots 655 streptavidin-conjugated (Thermo Fisher, Ref. Q10123MP). An important consideration in this step was the stoichiometry of the reaction. Each QD has 5-10 streptavidin molecules bound, and each streptavidin 3 available sites for binding biotin. To achieve a 1:1 ratio of QDs and antibodies, the reaction was carried out in the excess of biotin so it would fill the majority of sites and prevent binding of two or more antibodies per QD.

Conjugations with hAb and wAb were performed separately. Each time, three separate tubes were prepared to realize specific concentrations of reactive, namely hAb or wAb, biotin, and QDs. In each tube, 200 µl of a given reagent was prepared, 20 nM solutions of the antibody and QDs and 200 nM solution of biotin. Knowing starting concentrations and molecular weights, volumes of antibodies and QDs to add to achieve given ratios in 6% w/v Bovine Serum Albumin (BSA) were calculated, shown in Table 1. 6% w/v BSA solution was prepared beforehand, diluting 3g of BSA (Sigma, Ref. A7906) in 50 ml of PBS. Before pipetting QD stock, it was centrifuged at 10000 rpm for 4 min at 4ºC, and volume was carefully taken from the supernatant to avoid QD aggregations. QDs were always kept either on ice or in the fridge during the protocol.

Biotin was dissolved in DMSO to the final concentration of 200 nM, in multiple successive dilutions. In the last dilution, 2,4 µl of biotin in DMSO solution was mixed with 197,4 µl of 6% BSA in PBS to achieve 200 nM concentration of biotin in total volume of 200 µl. Lastly, all content from three tubes (with a specific antibody, QDs, and biotin) was mixed together in 1 tube, resulting in a total volume of 600 µl. Tube was covered in aluminum foil to preserve QD features and it was put in an ice box on an orbital shaker for 2h. One tube was made for each antibody (hAb and wAb).

Table 1. Concentrations and volumes of reagents for conjugation of biotinylated hAb fragments and whole antibody with streptavidin-coated QDs.

	hAb	QDs	wAb
Stock concentration	0.18 mg/ml	1 µM	0.5 mg/ml
Final concentration	20 nM	20 nM	20 nM
Volume of reactive	1.67 µl	4 µl	1.2 µl
Volume of 6% (w/v) BSA in PBS	198.33 µl	196 µl	198.8 µl
Total Volume	200 µl	200 µl	200 µl

2.2.4. Fixing and immunostaining

To determine the localization precision of the set-up and set a threshold for immobile movement for SPT experiments, cells were fixed in 2% paraformaldehyde (PFA). PFA terminates biological reactions and creates covalent cross-links between proteins, trapping them and limiting their movement. Immediately after fixing, cells were immunostained with antibodies conjugated with QDs. After seeding the plates, described in section 2.2.1., cells were incubated for a few days to reach desired confluency (70-80%). The first step was to remove medium and wash the cells 3x with 600 µl PBS, removing it in the last wash. Then the protocol was performed in 3 subsequent steps: fixing, blocking, and immunostaining. Blocking prevents unspecific binding of antibodies to molecules on the cell surface. Between each step, cells were washed with PBS as described.

Fixing was done by pipetting 200 µl 2% PFA to plates and incubating 15 min at room temperature and removing PFA. To block the unspecific bindings of antibody in the next step, 5 ml of blocking solution was prepared beforehand, consisting of 3% BSA, 2% human serum and 20 mM Glycine. The rest of the volume was filled with PBS. 200 µl of blocking solution was pipetted to plates, incubated for 1h at room temperature and removed.

Immunostaining of fixed cells was performed twice. Quantities of antibody conjugated with QDs were different depending on the experiment and antibody. The first time two plates were immunostained with the hAb-QD solution using 1/100 dilution in 6% BSA in PBS, adding 200 µl to each plate. The second time one plate was stained with hAb and two with the wAb-QD solution. Since the first time the fluorescence signal was too low and because the

conjugation was performed more than 1 month ago and possibly antibody degradation has started, the hAb-QDs solution was used as 1/5 dilution of stock. For the wAb, 1/50 stock dilution was used. For storing, 0.5-1ml of 2% PFA was added to plates, they were sealed with parafilm and placed in the fridge.

2.3. SINGLE-PARTICLE TRACKING

2.3.1. Single-Particle Tracking on fixed cells/Quantum Dots

Experiments on fixed cells were performed to obtain localization precision of the setup with cells and to set a reference for the movement observed for immobile integrins. The apparent diffusion measured with this experiment is due to parameters intrinsic to the experimental setup such as diffraction, limited photon flux, and camera pixelation. Microscope objective and plates were always cleaned with paper and 70% ethanol prior to microscopy. PFA was removed from plates under the protective hood. Plates were washed 3x times with 500 µl PBS. Since samples were immunostained with Ab-QD complex directly after fixation described in section 2.2.4., they were ready for observation after this step. Antibody dilutions are shown in Table 2. All videos of QDs on the membrane were captured by fluorescence microscope (Leica DMi8, Germany). Oil immersion objective (100X) objective was used in all experiments. Laser of 488 nm wavelength was used for excitation of QDs which have narrow, symmetric emission spectrum with the emission maximum near 655 nm. With the flexible microscope configuration, it was possible to easily switch from wide-field illumination (epifluorescence) to TIRF. A 6.7 ms exposure time of the camera and 20 ms frame acquisition time was used in imaging. Exposure time is the length of time when the digital sensor inside the camera is exposed to light. Frame acquisition time is the time difference between each subsequent frame in the video, also called time lag (Δt) which results in frame rate 1/0.02s or 40 fps (frames per second). Videos from experiment 1. had low QD fluorescent signal so samples from experiment 1. were imaged second time with less dilution.

Table 2. Scheme of the SPT experiments performed on integrins on fixed cells labeled with half-antibody and whole Ab. Ab dilution used in first imaging of the first experiment resulted in videos with too low QD signal so samples were imaged second time with less dilution.

	No. of samples	Passage number	Ab dilution	Exposure time (ms)	Δt (ms)	Frame rate (fps)
1.	2 x hAb	P7	*1st time:* 1/100 *2nd time*: 1/5	6.7	20	50
2.	3 (1x hAb, 2x wAb)	P10	*hAb*: 1/5 *wAb:* 1/50	6.7	20	50

Experiments on only QDs on glass were performed to obtain localization precision of the setup without cells. QDs were centrifuged (5 min, 4000rpm) and 1 µl was taken from the supernatant and pipetted to the tube with 999 µl PBS to make 1/1000 dilution. Dishes for observation of only QDs were coated with poly l-lysine. 200 µl of 0.1 % (w/v) in H_2O Poly-L-lysine solution (SIGMA, Ref. P8920) was added to each dish, covering the whole glass circle, and left in the incubator (37°C) for 10 minutes. The solution was then removed and the dish washed 3 times with 500 µl of PBS. After removing PBS, 500 µl of QD dilution was pipetted to the plate. To test the influence of the microscope settings on quantity and quality of trajectories, 8 videos with different microscope parameters were made, shown in Table 3.

Table 3. Eight different parameter combinations for videos of only QDs on the glass to test the influence of microscope settings on resulting trajectories.

	12bit videos			**16bit videos**	
	Exp.time(ms)	**Δt (ms)**		**Exp.time**	**Δt (ms)**
1.	6.7	20	**5.**	1	26
2.	11.7	25	**6.**	10	35
3.	16.7	35	**7.**	20	45
4.	26.7	45	**8.**	20	45

2.3.2. Single-Particle Tracking on living cells

Experiments on living cells were performed 2-3 days after seeding the plates when cells would reach approximately 80% confluency. Media from plates was then removed carefully with a pipette and cells washed 3x with PBS containing Ca^{2+} with 6% BSA. Then 200 µl of antibody was added to plates in different dilutions shown in Table 4. Plates were incubated for 15 minutes, then the antibody was removed and cells washed in the same way. Finally, 500 µl of PBS (Ca^{2+}) with 6% BSA was added to plates so cells would not dry out during observation and there is enough liquid to achieve TIRF. Cells were first imaged and focused in the bright field then in fluorescence mode. Before filming each video, a bright-field image was taken to make sure the area with cells is being filmed. Approximately 15-20 videos were filmed per sample.

Table 4. Scheme of the SPT experiments performed on integrins labeled with half-antibody and whole Ab.

	No. of samples	Passage number	Ab dilution	Exposure time (ms)	Δt (ms)	Frame rate (fps)
Half-Antibody (hAb)						
1.	4	P10	1/20	6.7	20	50
2.	4	P12	*Sample 1*: 1/20 *Sample 2-4:* 1/10	6.7	20	50
3.	3	P16	*Sample 1:* 1/10 *Sample 2-3:* 1/8	11.7	25	40
Whole Antibody (wAb)						
1.	4	P13	1/50	6.7	20	50
2.	4	P9	*Sample 1*: 1/20 *Sample 2-4:* 1/50	6.7	20	50
3.	3	P16	1/50	11.7	25	40

2.3.3. Video analysis

There are several free programs for single-particle tracking available online. Two were evaluated for the analysis of the results of experiments in this thesis: Mosaic (Sbalzarini and Koumoutsakos 2005) and TrackMate (Tinevez et al. 2017). Both are available as plugins for ImageJ/Fiji, free image-processing software and are easy-to-use, automated tools for particle tracking.

Videos were stored on the computer connected to the microscope. Since their size was large and transferring them was difficult, they were analyzed directly from that computer. Instead with Mosaic/TrackMate, in the end, videos were analyzed with MATLAB script "MTT" with a tracking algorithm implemented from Sergé *et al.*, 2008. Tracking process was time-consuming, and the great advantage of "MTT" script was that all videos of a single experiment could be left analyzing overnight or during the weekend. Another advantage was compatibility with other scripts written in MATLAB that were used for subsequent analysis of trajectories, for example, a script that calculates localization precision of the microscope setup. Importantly, the algorithm also takes into consideration QD blinking. Different values were tested for several parameters, before opting for the optimal values based on the results:

- r_0 - Gaussian radius in pixels was set to 1.5 pixels
- τ_{off} - disappearance probability (exponential decay) for blinking was set to -15 frames
- D_{max} - maximum diffusion coefficient was set to 0.7
- seuil_alpha – parameter for validation of pre-detected particles and new ones was set to 11

The result of the tracking was a text file for each video containing information about trajectories: trajectory number, x and y coordinates in each frame, average, minimum and maximum intensity of the signal. After tracking, trajectories were visually inspected with another MATLAB script called "anal_traj_v2". This script visually simulated trajectories from text files data in a user-friendly interface: with a slider, it was possible to go through each frame of the trajectory and decide with a "yes/no" button to keep or reject the trajectory. Trajectories less than 20 frames and trajectories with more than 50% of missing frames (frames in which the particle wasn't detected but algorithm was still able to reconnect the trajectory) were

excluded by this script because short trajectories and lack of particle detection could result in misleading data. Along with the graphical display of trajectory, on the same window were shown two plots: 1) MSD in relation to Δt, where Δt is the time difference between each frame and 2) average signal intensity in each frame. MSD is a measure of the average square distance between the start position and the end position of a particle for all time lags (t_{lag}), i.e. time distance between two points, in the trajectory. It is expressed by the formula:

$$MSD(t_{lag} = m\Delta t) = \frac{1}{N-m}\sum_{i=1}^{N-m}(x(t_i + m\Delta t) - x(t_i))^2,$$

where N is the number of points in the trajectory, x is a particle position observed at different time t_i. Selecting the pairs of points along the trajectory in respect to different time intervals is shown in Figure 7. Since time distance between each frame in this case is 0.02s, time interval 1 (1x Δt) is 0.02s, time interval 2 (2x Δt) is 0.04s, interval 3 (3x Δt) 0.06s and so on. To get the diffusion coefficient, MSD/nΔt plot was fitted with linear regression for only first 4 points because MSD curve at large t_{lag} has poor statistics (Manzo and Garcia-Parajo 2015). Diffusion coefficient (D) was then calculated from the slope of the fitted line, using equation MSD = 4*D*t_{lag}, where t_{lag} = n Δt. It is important to note that MSD represents an averaged characterization of the particle's trajectory. Therefore, it doesn't represent a good fit when one particle changes from one type of movement to another (e.g. slow to fast diffusion). Every trajectory was manually inspected. Reasons for rejection were:

1. Observation of two or more particles mixing paths or being too close so it was not possible to separate one from the other, which could be seen on trajectory display.
2. Observation of clearly immobile particle making large, isolated jumps which could happen because of the wrong reconnection due to blinking or to the low signal-to-noise ratio.
3. Observation of particle changing viewing planes (diameter becomes wider) or going out of focus. Measuring diffusion of a particle that is not tracked in the same horizontal plane would be misleading.
4. Observation of internalization (integrins being engulfed by the membrane to the inside of the cell). This could be seen on trajectory display as a fast motion along one line, and on the MSD/nΔt plot as the exponential curve. Internalization would usually start to happen when cells were observed for longer periods of time.

5. Trajectories with very low average intensity values because the localization precision, in this case, is most likely low.

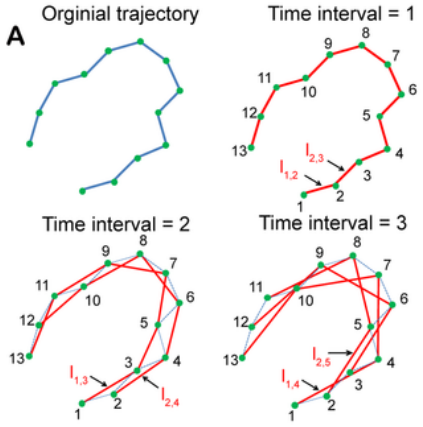

Figure 7. Points of trajectory selected for MSD calculation in relation to different time intervals (mΔt). For time interval 1 (mΔt = 0.02), the difference of points that are separated 0.02 s is calculated and squared, then the same is repeated for the next two points until the end. For time interval 2 we take the difference of points separated by 0.04, repeat the process and so on for time interval 3,4…

Two text documents were obtained after video analysis, with information about trajectories that remained after filtration (trajectory number, coordinates for x and y-axis, average intensity, diffusion and number of frames in which the particle was detected). Localization can only be estimated with certain error because of several reasons, some of which are because emission and detection of photons are stochastic processes, because of the presence of the background noise and because particles move within the solution (Manzo and Garcia-Parajo 2015). This error can be expressed as localization precision. Localization precision is a standard deviation of the estimated particle position in a given frame from the mean of total localizations estimated for the same particle (Deschout et al. 2014). With another script called "diagnostic", localization precision was calculated and plotted for each point with the equation:

$$\sigma_{xy} = \sqrt{\frac{1}{n-1}\sum_{i=1}^{n}\left(x_{p,i} - \bar{x}_p\right)^2} + \sqrt{\frac{1}{n-1}\sum_{i=1}^{n}\left(y_{p,i} - \bar{y}_p\right)^2},$$

where n is the number of frames where trajectory appears, and x_p and y_p particle's coordinates in a given frame, while $\bar{x}_p$ and $y_p$being the mean of all positions. Localization

precision of x-axis was plotted against the localization precision of y-axis to verify there are no great differences in precision between axes. The final plot was localization precision vs. square root of the number of photons. The number of photons was calculated by the formula:

$$number\ of\ photons = \frac{intensity(x) * (-e)/ADU}{QE}$$

where (-e)/ADU represents gain, camera parameter, which was 0.5 (-e)/ADU, and QE means quantum efficiency i.e. incident photon to converted electron ratio, which was 0.85. Aim of this plot was to verify that localization precision was decreasing with decreasing number of photons and that camera is working properly.

2.4. STATISTICAL ANALYSIS

To compare the diffusion of mobile integrins labeled with hAb to those labeled with wAb, Wilcoxon-Mann-Whitney Rank Sum two-tailed test was performed. Diffusion was compared separately for experiments with 50 and 40 frames per second frame rate with the level of significance $p<0.05$. To test for whether the proportions of immobile and mobile trajectories differ in cells of different passage number, 3-sample z-test for equality of proportions was performed. Test was done separately for hAb-labeled and wAb-labeled integrins, and each time for mobile, then immobile trajectories.

3. RESULTS

3.1. CELL CULTURE

Cell culture of human dermofibroblast cells was successfully established and maintained by splitting cells into new generations every 2-4 days. Cells were in good condition up to approximately 25th passage, but as time progressed their growth was much slower. There was also the difference in the cell morphology: older cells were greater in size and flatter than younger.

3.2. SINGLE-PARTICLE TRACKING ON FIXED CELLS

Experiments on fixed cells did not have conclusive results. In all experiments, using both hAb and wAb, there was a little amount of QD and most of the signal was coming from cell autofluorescence. Videos resulted in a very low number of short trajectories and therefore were not taken into consideration. This step needs further investigation.

3.3. DIFFUSION OF QUANTUM DOTS ON THE GLASS

2368 trajectories were tracked from videos of quantum dots fixed on glass. Videos were filmed with different microscope parameters described in Section 2. Comparison of mean values of the results of each video is shown in Table 5. It is worth noting that on the MSD/nΔt plot, multiple trajectories showed an unusual sinusoidal pattern. This pattern was observed in video 1 that was imaged with 6.7 ms exposure time and a similar pattern was observed in video 5. filmed with 16.7 ms exposure time. MSD/nΔt plots of trajectories in other videos showed no pattern. Mean diffusion range was from 9.76E-05 to 1.03E-03. Distribution of diffusion coefficients for all 8 videos is shown in Figure 8.

Table 5. Mean values of diffusion coefficient, trajectory length and number of frames in which the particle was detected (Number of frames ON) for each video. Videos were filmed on QDs fixed onglass with different microscope parameters, described in section 2.

Video number	Diffusion (μm^2/sec)	Trajectory length	Number of frames ON	Localization precision
1	9.10E-05	259.8571	224.424	0.0365
2	1.94E-04	250.8222	215.6578	0.0401
3	6.38E-04	323.8826	290.697	0.0288
4	2.53E-04	303.7043	272.2326	0.0350
5	1.03E-03	227.0214	166.0856	0.0362
6	9.76E-05	241.6391	197.2342	0.0279
7	1.69E-04	296.6738	261.4171	0.0348
8	1.01E-04	220.4188	185.2815	0.0281

Diffusion shown on histograms in this thesis is logarithmically scaled. To visualize negative and 0 values on a logarithmic scale, they were set to the minimum value of the diffusion coefficient greater than 0, which was a value very close to 0 in all cases. This was done strictly for visualization purpose, and all the statistics are carried out on the original dataset. 95^{th} percentile (with the value of 0.0011 $\mu m^2/s$) of distribution of diffusion coefficient was taken as a reference for immobile particles: everything less than this value was considered immobile. Mean trajectory length was from 220 to 324 frames. Distribution of trajectory length for all eight videos is shown in Figure 9. Mean localization precision was from 0.0279 to 0.0401 μm (Table 6).

Table 6. Mean localization precision of the microscope setup measured on QDs on the glass.

Video number	Mean localization precision (μm)
1.	0.0365
2.	0.0401
3.	0.0288
4.	0.0350
5.	0.0362
6.	0.0279
7.	0.0348
8.	0.0281

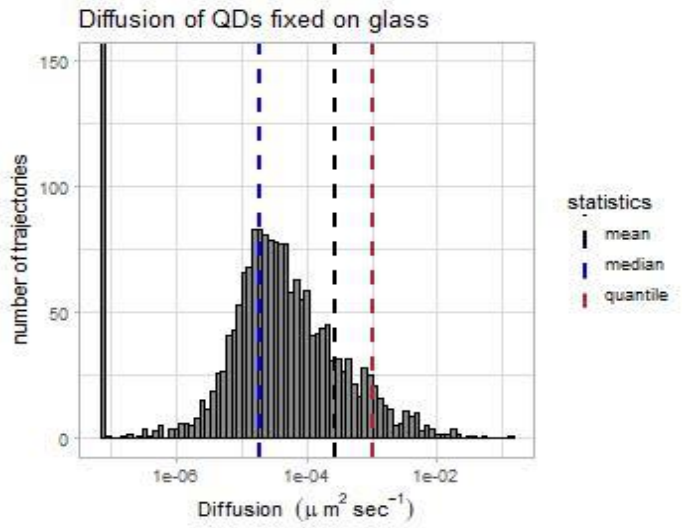

Figure 8. Distribution of diffusion coefficients of Quantum dots fixed on glass. Results were scaled logarithmically for visualization purpose. Mean diffusion was 2.7e-04 $\mu m^2/s$, median 1.9e-05 and 95^{th} quantile ~1e-03.

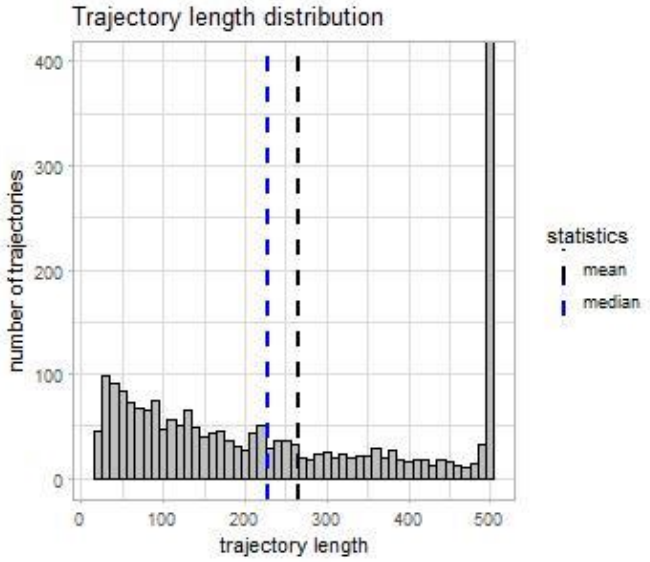

Figure 9. Distribution of trajectory length for all 8 videos of QDs on the glass. Mean trajectory length is 264.8611 frames, median 227.5 frames.

The plot which compares the localization precision of both axes is shown in Figure 10. Data shows that localization precision nearly symmetric along x and y-axes and follows a linear line. Localization precision in relation to the number of photons is shown on a plot in Figure 11. Precision is decreasing exponentially with the square root of the number of photons which is a good indication that the microscope setup is working properly. Plots originate from video 7. but the same pattern is observed in all videos.

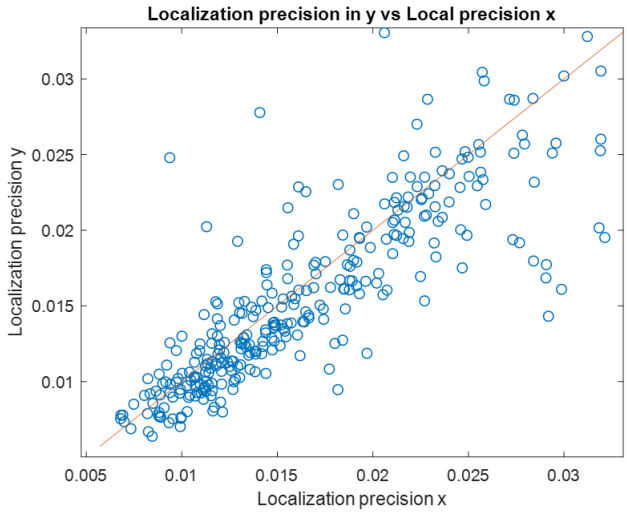

Figure 10. Localization precision in y-axis in relation to localization precision in x from results of video 7. (12bit, 20s exposure time, 45ms frame acquisition time).

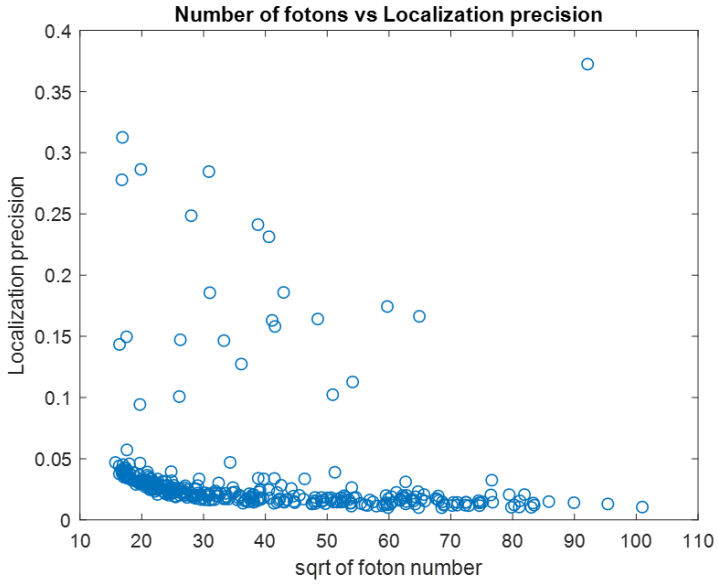

Figure 11. Localization precision in relation to photon number.

3.4. DIFFUSION OF INTEGRINS LABELED WITH HALF-ANTIBODY

A total of 7408 trajectories were tracked from videos of integrins labeled with hAb-QD complex with MTT script: 3693 trajectories from videos with filmed with 6.7 ms exposure time and 50 fps frame rate and 3715 trajectories from videos filmed with 11.7 ms exposure time and 40 fps frame rate. Each video consisted of 500 frames. On Figure 12. is shown an example of the immobile and mobile trajectory and an example of trajectories with mixed paths. It is important to separate results filmed with different microscope settings, mainly because the frame acquisition time parameter is used in the calculations of diffusion coefficients. Distribution of diffusion coefficients is shown in Figure 13. Results from the frame rate of 40 fps had a greater peak in immobile trajectories than results from 50 fps frame rate. MSD/nΔt plots of trajectories in videos imaged with 6.7 ms exposure time again showed the same sinusoidal pattern as QDs on glass but were not observed in videos imaged with 11.7 ms exposure time.

A) B)

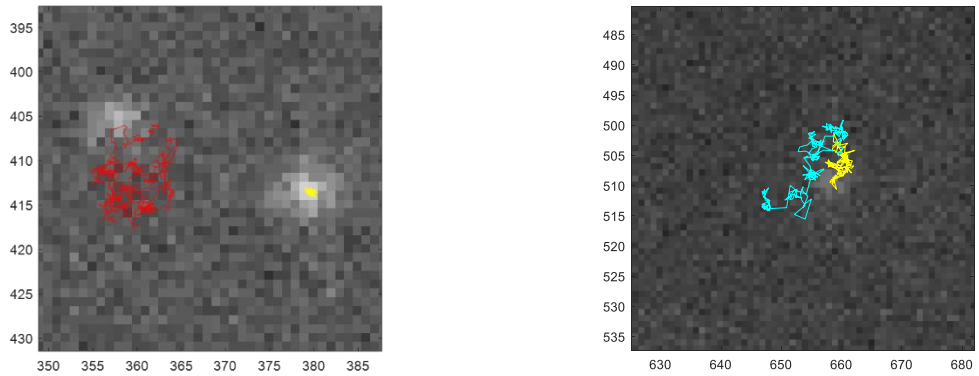

Figure 12. A) An example of a mobile trajectory (red) and immobile (yellow). B) shows two trajectories mixing paths which means that either two particles came too close one another or that the algorithm lost track of the particle and started new trajectory in later frames.

The distribution of diffusion coefficients was plotted separately for three types of cells of different passage number (the number of times the cells have been split into new generations): P10, P12 and P16 cells (Figure 14). In P10 cells, there is no significant difference in the immobile and the mobile part of the plot. From P12 to P16 cells, an increase in the immobile portion of the particles is observed as well as a decrease in the mobile portion.

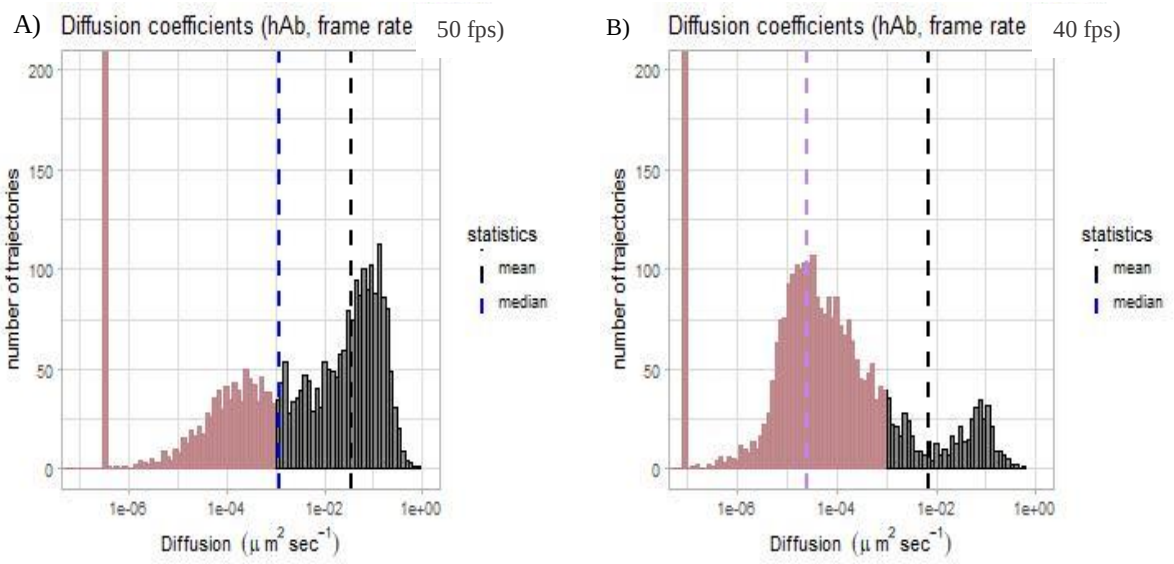

Figure 13. Distribution of diffusion coefficients measured from resulting trajectories of SPT experiments on living cells labeled with hAb. Part of the plot in pink represents all the diffusion coefficients less than 95%th percentile of the distribution of diffusion coefficients of QDs fixed on glass. This part is considered immobile, and grey part mobile. A) 3639 particle trajectories imaged with 6.7ms exposure time and 50 fps frame rate. Mean diffusion is 0.035s, median 0.0012s. B) 3715 particle trajectories imaged with 11.7ms exposure time and 40 fps frame rate. Mean diffusion is 0.0069, median 2.56554e-05s.

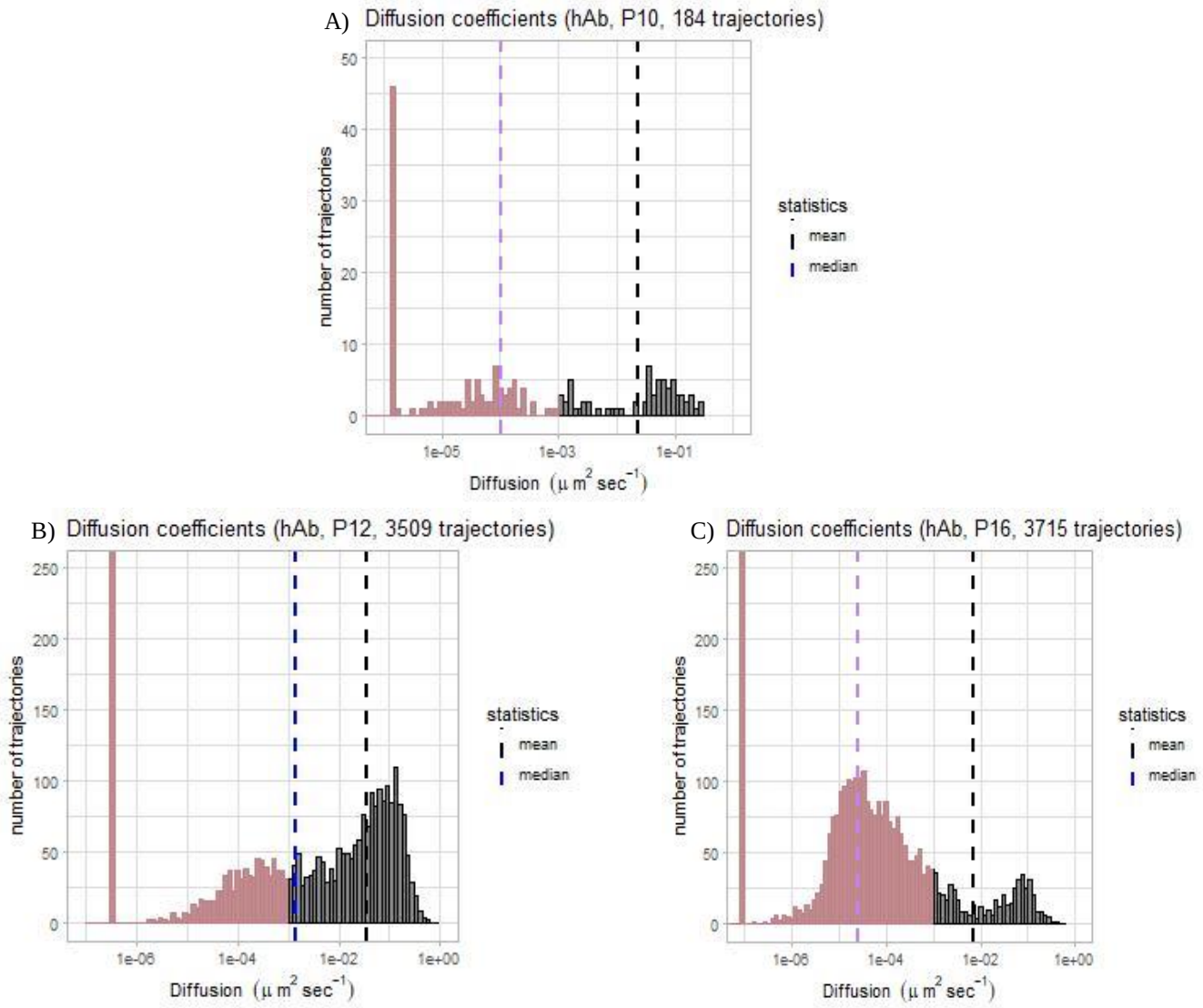

Figure 14. Distribution of diffusion coefficients measured from resulting trajectories of SPT experiments on living cells labeled with hAb, plotted by different passage number of the cells. Part of the plot in pink represents all the diffusion coefficients less than 95%th percentile of the distribution of diffusion coefficients of QDs fixed on glass. This part is considered immobile, and grey part mobile. A) Distribution of diffusion from 184 trajectories from experiments on cells that were passed 10 times i.e. were passage number P10. B) Distribution of diffusion from 3509 trajectories from experiments on P12 cells. C) Distribution of diffusion from 3715 trajectories from experiments on P16. From B) to C) an increase in immobile trajectories is observed as well as a decrease in mobile ones.

3.5. DIFFUSION OF INTEGRINS LABELED WITH WHOLE-ANTIBODY

A total of 11983 trajectories were obtained from results of SPT experiments on cells labeled with wAb: 8590 trajectories from videos imaged with 6.7 s exposure time and 50 fps frame rate and 3393 from videos imaged with 11.7 exposure time and 40 fps frame rate. Distribution of diffusion coefficients is shown in Figure 15. Frame rate of 40 fps results had a greater peak in immobile trajectories than results from 50 fps. Again, MSD/nΔt plots of trajectories in videos imaged with 6.7 ms exposure time again showed the pattern and were not observed in videos imaged with 11.7 ms exposure time. The distribution of diffusion coefficients plotted by passage number of the cells is shown in Figure 16. From P9 to P16, an increase in immobile trajectories is observed as well as a decrease in mobile ones.

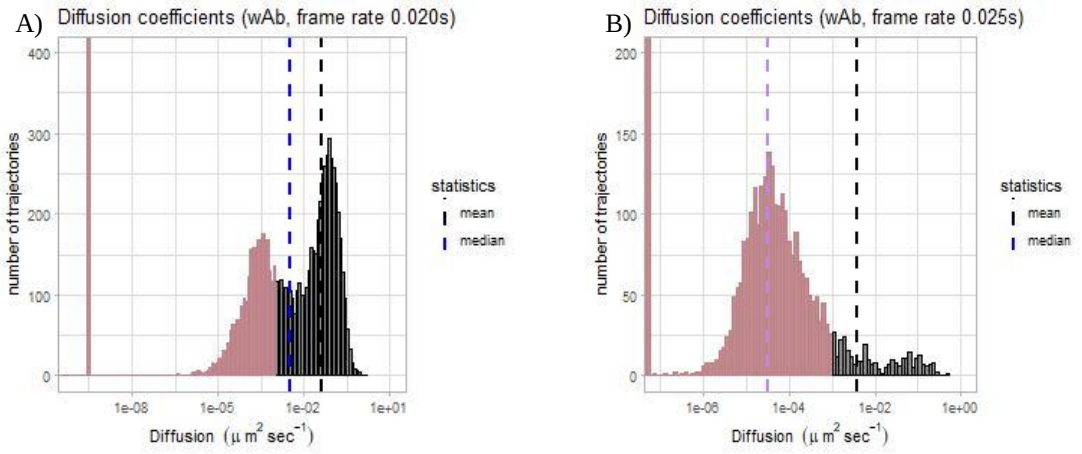

Figure 15. Distribution of diffusion coefficients measured from resulting trajectories of SPT experiments on living cells labeled with wAb. Part of the plot in pink represents all the diffusion coefficients less than 95%th percentile of the distribution of diffusion coefficients of QDs fixed on glass. This part is considered immobile, and grey part mobile. A) 8590 particle trajectories imaged with 6.7ms exposure time and 50 fps frame rate. Mean diffusion is 0.0412s , median 0.0034s. B) 3393 particle trajectories imaged with 11.7ms exposure time and 40 fps frame rate. Mean diffusion is 0.0036a, median 3.224894e-05s.

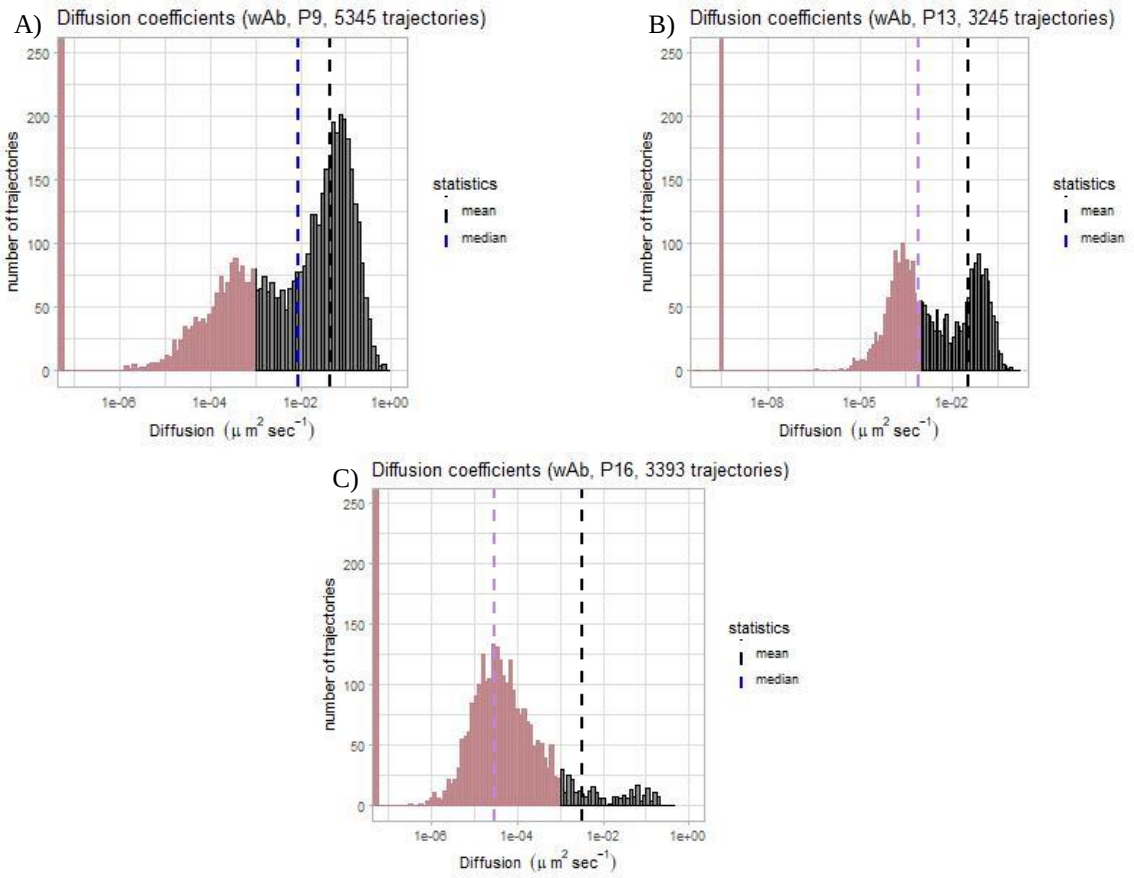

Figure 16. Distribution of diffusion coefficients measured from resulting trajectories of SPT experiments on living cells labeled with wAb, plotted by different passage number of the cells. Part of the plot in pink represents all the diffusion coefficients less than 95%th percentile of the distribution of diffusion coefficients of QDs fixed on glass. This part is considered immobile, and grey part mobile. A) Distribution of diffusion from 5345 trajectories on P9 cells. B) Distribution of diffusion from 3245 trajectories on P13 cells. C) Distribution of diffusion from 3393 trajectories on P16 cells. From A) to C) an increase in immobile trajectories is observed as well as a decrease in mobile ones.

3.6. STATISTICAL ANALYSIS

Diffusion of mobile integrins labeled with hAb and those labeled with wAb was compared with the Wilcoxon rank sum test with a level of significance $p<0.05$ (Table 7). For experiments filmed with 50 fps frame rate, a statistically significant difference in the two distributions was not determined, but was for experiments with 40 fps frame rate.

Table 7. Two-tailed Wilcoxon rank sum test on the distribution of diffusion coefficients of mobile hAb and wAb labeled integrins.

	50 fps frame rate	40 fps frame rate
hAb	1880 trajectories	511 trajectories
wAb	4991 trajectories	313 trajectories
p-value	0.8791	0.0001462

Equality of proportions of immobile and mobile trajectories in different cell passages was tested with a 3-sample z-test with a level of significance $p<0.05$. Data for the test is shown in Table 8. Ratios are shown graphically in Figures 17 and 18. There is a visible trend of decreasing of the mobile and increasing of the immobile proportions of trajectories with increasing cell 'age' or passage number with the exception of P10 cells with hAb-labeled integrins. P-value was $< 2.2e^{-16}$ in the testing of both immobile and mobile proportions in both hAb-labeled and wAb-labeled integrins.

Table 8. Ratios of mobile and immobile trajectories for each passage number, for hAb- and wAb-labeled integrins.

	hAb-labeled integrins				**wAb-labeled integrins**		
	P10	**P12**	**P16**		**P9**	**P13**	**P16**
mobile	67 (36%)	1813 (52%)	511 (14%)		3429 (64%)	1562 (48%)	309 (9%)
immobile	117 (64%)	1696 (48%)	3204 (86%)		1916 (36%)	1683 (52%)	3084 (91%)
total	**184**	**3509**	**3715**		**5345**	**3245**	**3393**

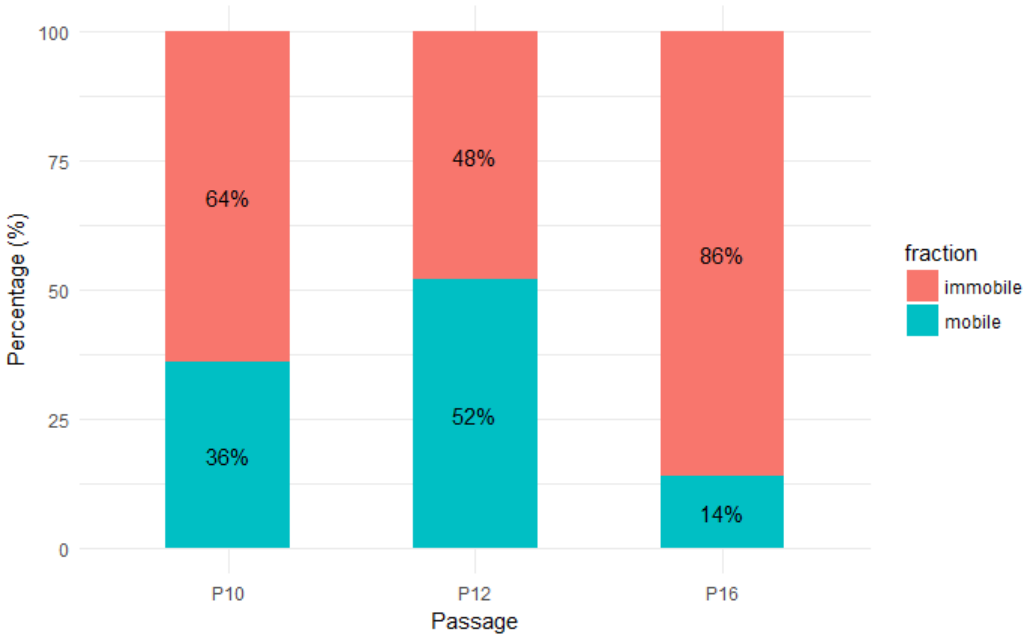

Figure 17. Mobile and immobile trajectories ratios of hAb-labeled integrins by different cell passage number. An increase of the immobile portion is visible from P12 to P16, although not from P10.

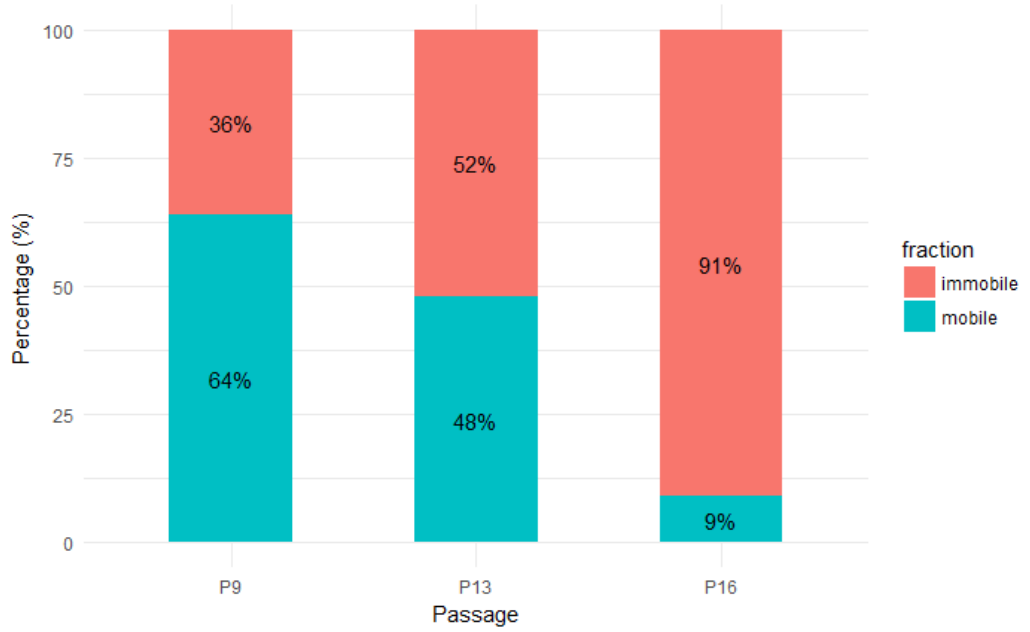

Figure 18. Mobile and immobile trajectories ratios of hAb-labeled integrins by different cell passage number. An increase in immobile fraction is observable with higher passage number.

4. DISCUSSION

In this study the diffusion of α5β1 integrin was measured from 7408 trajectories of integrins labeled with reduced half-antibody (hAb) and 11983 trajectories of integrins labeled with whole antibody (wAb). The difference in the distribution of diffusion coefficients due to different frame rates has been shown in both experiments with hAb and wAb (Figure 13. and 15.). However, it is important to note that in experiments of the 40 fps frame rate only P16 (highest passage number) cells were observed. With the increase of the cell senescence (cells with higher passage number), there was a notable decrease of mobile trajectories. Cells that were older showed the described trend in both hAb and wAb experiments (Figure 14. and 16., graphical display of the ratio of immobile and mobile trajectories shown on Figure 17. and 18.). In cells where integrins were labeled with hAb, the exception from the observed trend is a histogram of diffusion coefficients of P10 cells (Figure 13.) – there is not a clearly visible difference between the immobile and the mobile portion of the graph and it's an exception from the observed pattern. This is confirmed on Figure 17. where it is visible that the percentage of mobile trajectories is in fact increased from P10 to P12, and then decreased from P12 to P16. This exception from the pattern could partially be due to a low number of trajectories (184) of experiment on the P10 cells since it was among the first experiments done in this thesis and the protocol was still being optimized. When tested with the equality of proportions z-test, a significant difference was noted in mobile and immobile proportions of at least one sample (cells of different passage number) for both hAb- and wAb-labeled integrins. Therefore, the change in diffusion patterns of integrins seems to be related to the cell senescence.

In vitro primary fibroblasts exhibit senescence activity and decrease in growth rate with higher passage number (Hayflick and Moorhead 1961). They can undergo a limited number of cell divisions before entering senescent state. Young fibroblasts exhibit exponential growth, but with further passaging, more fibroblasts become cell cycle arrested and senescent (Schäuble et al. 2012). A decrease in growth rate was also noticeable in experiments carried out in this thesis, described in section 3.1. Other biological processes have been observed such as decreasing of the synthesis of the proteins of the ECM or increased degradation. With the degradation of collagen fibrils, fibroblast-ECM bonds become disrupted which causes lower mechanical force and less spreading on the surface (Cole et al. 2018). It has also been found by Magnuson et al. 1991. that the alternative splicing of fibronectin pre-mRNA is altered in *in*

vitro aging of primary fibroblasts. Moreover, there is a different gene expression profile related to the aging process of fibroblasts (Lago and Puzzi 2019) and a wide range of observed biochemical and genome changes (Tigges et al. 2014). Therefore, considering the described alterations of the ECM, and biochemical and genomic changes of the in vitro aged primary fibroblasts, it is possible that aging also affects the movement of integrins on the cell membrane. To analyze the effect of cell senescence on the diffusion rate of integrins, the study should be expanded to a greater number of samples from multiple cell generations.

A study by Rossier *et al.*, 2012 that also analyses the diffusion of integrins (β3 and β1 integrin) has similar results of the distribution of diffusion coefficients (outside focal adhesions) as the results of the experiments of this thesis when 50 fps frame rate was used in both hAb and wAb experiments. It is important to note that in the case of experiments conducted in this thesis, it was not evident whether the QDs that were tracked were inside or outside focal adhesions. The QD-antibody complex is relatively big and it was not clear whether it could pass from outside the cell in between the glass and the attached cell to reach focal adhesions. Therefore, the assumption is that the majority of the inspected trajectories were outside focal adhesions, from the apical part of the cell. The threshold value for immobile movement varies with different experimental set-ups, and in the mentioned study was 0.008 $\mu m^2/s$. In the other study of diffusion of α4β1 integrins on T cells by Sosa-Costa *et al.*, 2016, the threshold value was 0.025 $\mu m^2/s$ and 0.001 $\mu m^2/s$ in the study by Borgman *et al.*, 2014.

When tested with the Wilcoxon sum rank test, the diffusion of the mobile trajectories was statistically different for experiments with 40 fps frame rate but not for experiments with the 50 fps frame rate. Since the hypothesis was that the diffusion rate of wAb labeled integrins is changed due to artificial dimerization, observation of difference was in accordance with the expected results, although it is not clear why the difference is observed in mobile trajectories in only 40 fps frame rate videos. One improvement that could be made is to further separate particles to immobile and confined particles (those restricted to a small region), and those with directed, normal, and anomalous diffusion. This requires the use of complex mathematical calculations described by Schütz, Schindler and Schmidt, 1997 or novel approaches (Monnier et al. 2012; Slator, Cairo, and Burroughs 2015). Nevertheless, these observations indicate that the diffusion rate obtained for SPT experiments changes due to different immuno-labeling and that the step of the preferential reduction of the antibody to hAb fragments is advisable.

SPT experiments on the fixed cell were inconclusive, possibly because of paraformaldehyde-induced autofluorescence. Autofluorescence and noise are significant problems in SPT experiments since the sensitivity of the microscope is increased with higher resolution. It is shown that autofluorescence is often increased when using cross-linking fixatives such as paraformaldehyde and glutaraldehyde (Allen, Ross, and Davidson 2013). Some studies suggest washing samples with PBS containing 50 mM glycine to reduce the paraformaldehyde-induced autofluorescence (Allen, Ross, and Davidson 2013; Shaner et al. 2013). Background noise, on the other hand, was greatly decreased when imaging in TIRF mode. The problem of the low number of QDs observed on the samples of fixed cells needs further investigation.

With the SPT experiment on immobilized QDs on the glass, it was shown that the microscope setup was working properly, with mean localization precision between 28 and 40 nm. There was no notable difference in localization precision along x and y-axis (Figure 10) and localization precision was exponentially decreasing with the square root of photon number (Figure 11). This result is compatible with the fact that uncertainty in determining the position of the molecule is inversely scaled to the square root of the photon number (Xi 2014). Because of their optical properties such as the narrow emission spectra and high signal-to-noise ratio, Quantum Dots enable the spatial resolution of 10-15 nm (Wegner and Hildebrandt 2015; Manzo and Garcia-Parajo 2015). One example is the study by (Arnspang, Brewer, and Lagerholm 2012), where the localization precision of streptavidin-coated QD655 that have been immobilized on glass was 14 nm. Therefore, although the resolution from experiments in this thesis is greatly improved compared to the fluorescence microscopy methods where resolution is diffraction-limited and typically equals to 250 nm (for visible light and an NA of 1.3), there is still the possibility of improvement in this direction.

Multiple trajectories, from both the fixed QDs and living-cell experiments, tracked from videos imaged with 6.7 ms exposure time had an unusual sinusoidal pattern on MSD/nΔt plot. This effect was removed by using other values for exposure time, but the reason it occurred is still not clear. It is possible that the pattern is an artefact caused by the short exposure time incompatible with the way the camera reads the lines.

Finally, after the successful method implementation achieved in this study, the next step in the research of lateral diffusion of integrins would be the analysis of diffusion after adding certain ligands/stimulants that simulate different cell conditions as in the example in the studies by Borgman *et al.*, 2014; Sosa-Costa *et al.*, 2016. Another interesting topic is the integrin role in cancer progression (Guo et al. 2002; Hou et al. 2016).

5. CONCLUSIONS

- From SPT on QDs immobilized on glass, 2368 trajectories were tracked. Microscope set-up was shown to work properly. Reference for the immobile movement (set as the 95%-percentile of distribution of diffusion coefficients obtained from the experiment) was equal to 0.001 $\mu m^2/s$. Particles were localized with precision in the range 28 and 40 nm, far surpassing the precision from conventional microscopy methods, although improvements can be made to reach the precision in other studies on the topic.
- SPT on fixed cells has yielded no valid trajectories.
- 7408 trajectories were tracked from SPT experiments on living cells labeled with hAb-QD complex: 3693 trajectories from videos filmed with 6.7 ms exposure time and 50 frames per second frame rate and 3715 trajectories from videos filmed with 11.7 ms exposure time and 40 frames per second frame rate. 11983 trajectories were tracked from SPT experiments on cells labeled with wAb: 8590 trajectories from videos imaged with 6.7 s exposure time and 50 fps frame rate and 3393 from videos imaged with 11.7 exposure time and 40 fps frame rate. An increase of immobile portion of trajectories of integrins and a decrease of the mobile was observed in cells with higher passage numbers. Statistically significant difference in these portions was shown for different passage numbers in both hAb- and wAb-labeled integrins.
- The difference in the distribution of diffusion between hAb and wAb-labeled integrins was statistically significant in experiments with 40 fps frame rate, but not in experiments with 50 fps frame rate.

6. REFERENCES

Ahi, Kiarash, and Mehdi Anwar. 2016. “Developing Terahertz Imaging Equation and Enhancement of the Resolution of Terahertz Images Using Deconvolution.” In *Terahertz Physics, Devices, and Systems X: Advanced Applications in Industry and Defense*, 98560N. https://doi.org/10.1117/12.2228680.

Alberts, Bruce, Alexander Johnson, Julian Lewis, David Morgan, Martin Raff, Keith Roberts, and Peter Walter. 2017. *Molecular Biology of the Cell*. https://doi.org/10.1201/9781315735368.

Allen, John R., Stephen T. Ross, and Michael W. Davidson. 2013. “Sample Preparation for Single Molecule Localization Microscopy.” *Physical Chemistry Chemical Physics*, 43. https://doi.org/10.1039/c3cp53719f.

Arnspang, Eva C., Jonathan R. Brewer, and B. Christoffer Lagerholm. 2012. “Multi-Color Single Particle Tracking with Quantum Dots.” *PLoS ONE*, 7 (11): e48521. https://doi.org/10.1371/journal.pone.0048521.

Borgman, Kyra J E, Thomas S. Van Zanten, Carlo Manzo, Raquel Cabezón, Alessandra Cambi, Daniel Benítez-Ribas, and Maria F. Garcia-Parajo. 2014. “Priming by Chemokines Restricts Lateral Mobility of the Adhesion Receptor LFA-1 and Restores Adhesion to ICAM-1 Nano-Aggregates on Human Mature Dendritic Cells.” *PLoS ONE*, 9 (6): e99589 https://doi.org/10.1371/journal.pone.0099589.

Cole, Megan A., Taihao Quan, John J. Voorhees, and Gary J. Fisher. 2018. “Extracellular Matrix Regulation of Fibroblast Function: Redefining Our Perspective on Skin Aging.” *Journal of Cell Communication and Signaling*, 12 (1): 35-43. https://doi.org/10.1007/s12079-018-0459-1.

Deschout, Hendrik, Francesca Cella Zanacchi, Michael Mlodzianoski, Alberto Diaspro, Joerg Bewersdorf, Samuel T. Hess, and Kevin Braeckmans. 2014. “Precisely and Accurately Localizing Single Emitters in Fluorescence Microscopy.” *Nature Methods*, 11: 253–266. https://doi.org/10.1038/nmeth.2843.

Erez, Neta, Morgan Truitt, Peter Olson, and Douglas Hanahan. 2010. “Cancer-Associated Fibroblasts Are Activated in Incipient Neoplasia to Orchestrate Tumor-Promoting Inflammation in an NF-KB-Dependent Manner.” *Cancer Cell* 17 (2): 135–147. https://doi.org/10.1016/J.CCR.2009.12.041.

Groc, Laurent, Mathieu Lafourcade, Martin Heine, Marianne Renner, Victor Racine, Jean-Baptiste Sibarita, Brahim Lounis, Daniel Choquet, and Laurent Cognet. 2007. “Surface Trafficking of Neurotransmitter Receptor: Comparison between Single-Molecule/Quantum Dot Strategies.” *The Journal of Neuroscience : The Official Journal of the Society for Neuroscience*, 27 (46): 12433–37. https://doi.org/10.1523/JNEUROSCI.3349-07.2007.

Guo, Hua Bei, Intaek Lee, Maria Kamar, Steven K. Akiyama, and Michael Pierce. 2002. “Aberrant N-Glycosylation of B1 Integrin Causes Reduced A5β1 Integrin Clustering and Stimulates Cell Migration.” *Cancer Research*, 62 (23): 6837-45.

Hayflick, L., and P. S. Moorhead. 1961. “The Serial Cultivation of Human Diploid Cell Strains.” *Experimental Cell Research*, 25 (3): 585-621. https://doi.org/10.1016/0014-4827(61)90192-6.

Hermanson, Greg T. 2007. “Antibody Modification and Conjugation.” In book *Bioconjugate Techniques*, pp.783-823 . https://doi.org/10.1016/b978-012342335-1/50011-7.

Hou, Sicong, Tomoya Isaji, Qinglei Hang, Sanghun Im, Tomohiko Fukuda, and Jianguo Gu. 2016. “Distinct Effects of B1 Integrin on Cell Proliferation and Cellular Signaling in MDA-MB-231 Breast Cancer Cells.” *Scientific Reports*, 6, 18430. https://doi.org/10.1038/srep18430.

Hynes, Richard O. 2002. “Integrins: Bidirectional, Allosteric Signaling Machines.” *Cell* 110 (6): 673–87. https://doi.org/10.1016/S0092-8674(02)00971-6.

Kusumi, Akihiro, Chieko Nakada, Ken Ritchie, Kotono Murase, Kenichi Suzuki, Hideji Murakoshi, Rinshi S. Kasai, Junko Kondo, and Takahiro Fujiwara. 2005. “Paradigm Shift of the Plasma Membrane Concept from the Two-Dimensional Continuum Fluid to the Partitioned Fluid: High-Speed Single-Molecule Tracking of Membrane Molecules.” *Annual Review of Biophysics and Biomolecular Structure*, 34:351-378. https://doi.org/10.1146/annurev.biophys.34.040204.144637.

Lago, Juliana Carvalhães, and Maria Beatriz Puzzi. 2019. “The Effect of Aging in Primary Human Dermal Fibroblasts.” *Plos One* 14 (7): e0219165. https://doi.org/10.1371/journal.pone.0219165.

Magnuson, V. L., M. Young, D. G. Schattenberg, M. A. Mancini, D. Chen, B. Steffensen, and R. J. Klebe. 1991. “The Alternative Splicing of Fibronectin Pre-MRNA Is Altered during Aging and in Response to Growth Factors.” *Journal of Biological Chemistry*, 266 (22):14654-62.

Makaraviciute, Asta, Carolyn D. Jackson, Paul A. Millner, and Almira Ramanaviciene. 2016. “Considerations in Producing Preferentially Reduced Half-Antibody Fragments.” *Journal of Immunological Methods*, 429:50-56. https://doi.org/10.1016/j.jim.2016.01.001.

Manzo, Carlo, and Maria F. Garcia-Parajo. 2015. “A Review of Progress in Single Particle Tracking: From Methods to Biophysical Insights.” *Reports on Progress in Physics*, 78 (12): 124601. https://doi.org/10.1088/0034-4885/78/12/124601.

Meijering, Erik, Ihor Smal, and Gaudenz Danuser. 2006. “Tracking in Molecular Bioimaging.” *IEEE Signal Processing Magazine*, 23 (3):46-53. https://doi.org/10.1109/MSP.2006.1628877.

Monnier, Nilah, Syuan Ming Guo, Masashi Mori, Jun He, Péter Lénárt, and Mark Bathe. 2012. “Bayesian Approach to MSD-Based Analysis of Particle Motion in Live Cells.” *Biophysical Journal*, 103 (3):616-626. https://doi.org/10.1016/j.bpj.2012.06.029.

Nermut, M V, N M Green, P Eason, S S Yamada’, and K M Yamada’. 1988. “Electron Microscopy and Structural Model of Human Fibronectin Receptor.” *The EMBO Journal*, 7 (13):4093-4099. https://www.ncbi.nlm.nih.gov/pmc/articles/PMC455118/pdf/emboj00150-0076.pdf.

Nirmal, M., B. O. Dabbousi, M. G. Bawendi, J. J. Macklin, J. K. Trautman, T. D. Harris, and L. E. Brus. 1996. "Fluorescence Intermittency in Single Cadmium Selenide Nanocrystals." *Nature,* 383:802–804. https://doi.org/10.1038/383802a0.

Niu, Gang, and Xiaoyuan Chen. 2012. "Why Integrin as a Primary Target for Imaging and Therapy." *Theranostics,* 1:30-47. https://doi.org/10.7150/thno/v01p0030.

Noda, Ichiro, Shigeharu Fujieda, Mizue Seki, Nobuyuki Tanaka, Hiroshi Sunaga, Toshio Ohtsubo, Hideaki Tsuzuki, Guo Kang Fan, and Hitoshi Saito. 1999. "Inhibition of N-Linked Glycosylation by Tunicamycin Enhances Sensitivity to Cisplatin in Human Head-and-Neck Carcinoma Cells." *International Journal of Cancer*, 80 (2): 279–84. https://doi.org/10.1002/(SICI)1097-0215(19990118)80:2<279::AID-IJC18>3.0.CO;2-N.

Rossier, Olivier, Vivien Octeau, Jean-Baptiste Sibarita, Cécile Leduc, Béatrice Tessier, Deepak Nair, Volker Gatterdam, et al. 2012. "Integrins B1 and B3 Exhibit Distinct Dynamic Nanoscale Organizations inside Focal Adhesions." *Nature Cell Biology*, 14 (10): 1057–67. https://doi.org/10.1038/ncb2588.

Sbalzarini, I. F., and P. Koumoutsakos. 2005. "Feature Point Tracking and Trajectory Analysis for Video Imaging in Cell Biology." *Journal of Structural Biology,* 151 (2):182-195. https://doi.org/10.1016/j.jsb.2005.06.002.

Schäuble, Sascha, Karolin Klement, Shiva Marthandan, Sandra Münch, Ines Heiland, Stefan Schuster, Peter Hemmerich, and Stephan Diekmann. 2012. "Quantitative Model of Cell Cycle Arrest and Cellular Senescence in Primary Human Fibroblasts." *PLoS ONE,* 7 (8):e42150. https://doi.org/10.1371/journal.pone.0042150.

Schütz, G. J., H. Schindler, and Th Schmidt. 1997. "Single-Molecule Microscopy on Model Membranes Reveals Anomalous Diffusion." *Biophysical Journal*, 73:1073-1080. https://doi.org/10.1016/S0006-3495(97)78139-6.

Sergé, Arnauld, Nicolas Bertaux, Hervé Rigneault, and Didier Marguet. 2008. "Dynamic Multiple-Target Tracing to Probe Spatiotemporal Cartography of Cell Membranes." *Nature Methods*, 5:687–694. https://doi.org/10.1038/nmeth.1233.

Shaner, Nathan C, Gerard G Lambert, Andrew Chammas, Yuhui Ni, Paula J Cranfill, Michelle A Baird, Brittney R Sell, et al. 2013. "A Bright Monomeric Green Fluorescent Protein Derived from Branchiostoma Lanceolatum." *Nature Methods,* 10:407–409. https://doi.org/10.1038/nmeth.2413.

Slator, Paddy J., Christopher W. Cairo, and Nigel J. Burroughs. 2015. "Detection of Diffusion Heterogeneity in Single Particle Tracking Trajectories Using a Hidden Markov Model with Measurement Noise Propagation." *PLoS ONE,* 10 (10):e0140759. https://doi.org/10.1371/journal.pone.0140759.

Sosa-Costa, Alberto, Sol Isern De Val, Silvia Sevilla-Movilla, Kyra J.E. Borgman, Carlo Manzo, Joaquin Teixidó, and Maria F. Garcia-Parajo. 2016. "Lateral Mobility and Nanoscale Spatial Arrangement of Chemokine-Activated A4β1 Integrins on T Cells." *Journal of Biological Chemistry*, 291:21053-21062. https://doi.org/10.1074/jbc.M116.733709.

Sriram, Gopu, Paul Lorenz Bigliardi, and Mei Bigliardi-Qi. 2015. "Fibroblast Heterogeneity and Its Implications for Engineering Organotypic Skin Models in Vitro." *European Journal of Cell Biology*, 94 (11):483-512. https://doi.org/10.1016/j.ejcb.2015.08.001.

Tigges, Julia, Jean Krutmann, Ellen Fritsche, Judith Haendeler, Heiner Schaal, Jens W. Fischer, Faiza Kalfalah, et al. 2014. “The Hallmarks of Fibroblast Ageing.” *Mechanisms of Ageing and Development,* 138:26-44. https://doi.org/10.1016/j.mad.2014.03.004.

Tinevez, Jean Yves, Nick Perry, Johannes Schindelin, Genevieve M. Hoopes, Gregory D. Reynolds, Emmanuel Laplantine, Sebastian Y. Bednarek, Spencer L. Shorte, and Kevin W. Eliceiri. 2017. “TrackMate: An Open and Extensible Platform for Single-Particle Tracking.” *Methods,* 115:80-90. https://doi.org/10.1016/j.ymeth.2016.09.016.

Wegner, K. David, and Niko Hildebrandt. 2015. “Quantum Dots: Bright and Versatile in Vitro and in Vivo Fluorescence Imaging Biosensors.” *Chemical Society Reviews,* 44 (14):4792-4834 . https://doi.org/10.1039/c4cs00532e.

Xi, Peng. 2014. *Optical Nanoscopy and Novel Microscopy Techniques*. https://doi.org/10.1201/b17421.

7. CURRICULUM VITAE

Jelena Ivčević Date of birth: 23 February 1995

Education:

1. Faculty of Science and Technology, Universitat de Vic – Universitat Central de Catalunya
   Erasmus + internship project at Quantitative Bioimaging Research group (QuBi lab)
   2018 – 2019

2. Faculty of Science and Technology, Universitat de Vic – Universitat Central de Catalunya
   Erasmus + student exchange at Biotechnology degree
   2017-2018

3. Department of Biology, Faculty of Science, University of Zagreb
   Master's degree in Molecular Biology
   2016-2019

4. Department of Biology, Faculty of Science, University of Zagreb
   Bachelor's degree in Biology
   Thesis: "Epigenetics and evolution"
   2013-2016

5. V Gymnasium – Vladimir Nazor, Split
   2009 – 2013

Experience:

1. Department of Biochemistry, Faculty of Medicine, Split,
   Volunteer in cell culture laboratory with a PhD-student
   August 2014 – September 2014

2. Division of Animal Physiology, Department of Biology, Faculty of Science, University of Zagreb
   Laboratory professional training
   Mentor: doc. dr. sc. Sofia Ana Blažević
   March 2016. – June 2016.

3. Volunteer at scientific manifestation "Biology Night", University of Zagreb, Faculty of Science, Department of Molecular Biology

Personal skills:

Languages:

- Active use of English language (C1 – proficient user)
- A1 in Spanish language (basic user)

Computer literacy:

- Proficient user of MS Office programs (Word, Excell, Acess, Power Point)
- Independent user of R-programming language
- Basic knowledge of Python- programming language
- Basic knowledge of MatLab programming language
- Independent user of ImageJ program